INDIAN JOURNAL OF SCIENCE AND TECHNOLOGY

RESEARCH ARTICLE

Check for updates

OPEN ACCESS

Received: 05-11-2024

Accepted: 27-11-2024

Published: 17-12-2024

Citation: Rajasekar G, Guru Sami K (2024) Resistance Spot Welding: Surface Appearance Image-Based Weld Quality Prediction using HCLAN. Indian Journal of Science and Technology 17(46): 4808-4818. https://doi.org/10.17485/IJST/v17i46.3606

* **Corresponding author**.

graju1983@gmail.com

Funding: None

Competing Interests: None

Published By Indian Society for Education and Environment (iSee)

ISSN
Print: 0974-6846
Electronic: 0974-5645

Resistance Spot Welding: Surface Appearance Image-Based Weld Quality Prediction using HCLAN

G Rajasekar[1]*, K Guru Sami[2]

1 Research scholar, Department of Manufacturing Engineering, St Peters Institute of Higher Education and Research, Avadi, Chennai, Tamil Nadu, India
2 Associate Professor, Department of Mechanical Engineering, St. Peter's Institute of Higher Education and Research, Avadi, Chennai, Tamil Nadu, India

Abstract

Objectives: This study enhances resistance spot welding (RSW) quality inspection by proposing an automated method to predict weld quality, minimizing reliance on manual evaluation. **Methods:** A Hybrid CNN-LSTM with Attention Network (HCLAN) was developed, leveraging heat trace (HT) images of the weld surface for quality forecasting. Experiments used advanced high-strength steel (AHSS, 980 MPa) and uncoated cold-rolled (CR) steel, measuring tensile shear strength (TSS), weld fracture mode, nugget diameter, and ejection occurrence. **Findings:** The HCLAN model achieved a nugget diameter prediction error of 2.8% and TSS prediction error of 2.3%. For weld fracture mode and expulsion detection, it achieved 100% classification accuracy. **Novelty:** The integration of CNN, LSTM, and attention mechanisms in HCLAN demonstrates a novel approach to automating weld quality assessment. This method significantly reduces inspection errors and enhances efficiency in industrial welding processes.

Keywords: Resistance spot welding; Tensile shear strength; Nugget size; Surface appearance image; Weld quality; CNN-LSTM

1 Introduction

Resistance spot welding (RSW) is one of the most widely adopted joining techniques for sheet metal components, particularly in the automotive industry, due to its exceptional strength-ductility combinations and cost efficiency. Advanced high-strength steels (AHSSs) are extensively used in structural components of modern automobiles, where RSW plays a critical role. This welding method is also versatile, finding applications in diverse industries such as automotive manufacturing, electrical equipment, rail cars, precision instruments, and aerospace[1–7]. Its benefits include high efficiency, ease of use, low operational costs, and minimal noise. However, achieving consistent welding quality in practical applications remains a significant challenge. Even with standardized process parameters, several complex and interacting factors, such as material properties, equipment conditions, and process variations, lead to fluctuations in weld quality. These inconsistencies can compromise structural integrity and performance, highlighting the critical need for effective quality evaluation methods.

Various techniques have been explored to assess and control weld quality, including destructive and nondestructive testing. Destructive testing methods, such as tensile shear and peel tests, are widely used due to their reliability in identifying weld defects such as ejection and undersized welds [8]. However, these methods are limited in their practicality for large-scale production due to their high costs, inefficiency, and inability to diagnose faults in real time [9]. On the other hand, nondestructive testing (NDT) methods, which leverage diverse process features, have shown promise in addressing these limitations by offering efficient and real-time quality assessment. Despite their potential, the efficacy of NDT methods is not universally established across varying manufacturing conditions, leaving a research gap in optimizing and validating these techniques. This study aims to address these gaps by proposing an innovative approach to improve the evaluation and control of weld quality in RSW. Specifically, the proposed method combines advanced nondestructive testing techniques with data-driven insights to overcome the limitations of existing practices. The advantages of the proposed method, such as improved real-time fault detection, cost-effectiveness, and scalability for industrial applications, will be demonstrated and compared against existing approaches. Through systematic experimentation and validation, this research seeks to establish a robust framework for enhancing weld quality assurance, ultimately contributing to the advancement of RSW processes in industrial settings.

Numerous studies have been done on the subject of nugget size and appearance since they are major factors in determining the mechanical assets of an RSW welding spot. Ao et al. [10] measured the remaining pressure of the RSW joint using a unique X-ray diffraction technique. The compressing pressure and the electrode force are the primary factors causing deformation, according to Liu et al.'s [11] investigation of the RSW distortion parameters using finite element analysis. Liquid metal embrittlement (LME) in RSW was investigated by Ma et al. [12] in order to determine the variables influencing weld fracture. In order to investigate the connection among dynamic resistance and welding quality, Zhao et al. [13] collected features from the active RSW signals and developed a scientific model. The findings indicated that the current is the most important element. In order to overcome the issue of composite products poor welding performance. Burca et al.'s [14] investigation looked at how process variables affected RSW indentation depth. It is evident that signals and process factors were primarily used in nugget quality research studies to quantify the mechanical characteristics of RSW. Nevertheless, the appropriate research on appearance quality cannot be conducted effectively using RSW appearance image data. Because an RSW welding spot's appearance quality primarily reflects issues with the welding process, there isn't a lot of research on the subject because of its characteristics, which include high randomness, irregularities, and appearance categories. Since faulty appearances are frequently associated with welding locations with poor mechanical qualities, some nugget defects can be identified early on using appearance detection. However, at the moment, the body-in-white's RSW appearance quality is primarily determined by manual examination. As a result, there is an urgent need for an effective automated recognition approach to enable real-time inspection and feedback.

One effective nondestructive verifying technique for quality checks has been visual examination. A vision method, which essentially comprises of cameras and a computer with specialized image-processing application, can automate this procedure. Ye et al. [15] created a vision scheme that uses a neural network that has been trained to abstract fifteen attributes from welding photos and identify weld flaws. In order to classify the spot welding, a pre-trained model was used by Yang et al. [16] to extract properties from weld spot pictures. Artificial neural networks (ANN) were the image processing technique employed by Bacioiu et al. [17] to assess tungsten inactive gas joining using a high active range camera. In order to create a smart diffusion monitoring system for gas tungsten arc welding, Chen et al. [18] combined the supervised machine learning approach with the visual feature abstraction technique, and Nomura et al. [19] used a deep learning methodology to predict the weld depth. A novel online flaw detection method for aluminum mixture in machinelike arc fusing, based on the Convolutional Neural Network (CNN) model, was presented by Zhang et al. [20]. Wang et al. [21] used a CNN model to predict the back-side bead width from top-side pictures, demonstrating the application of deep learning in the industrial setting through a case study of welding quality prediction. CNN-based techniques investigate the nugget surface's spatial properties for quality prediction, but they do not completely take use of the temporal variations. LSTM is able to capture temporal dependencies and patterns over several frames/images shown in Table 1. Therefore, this proposed work used HCLAN for quality prediction of RSW.

Table 1. Summary of Key Approaches and Limitations in Welding Research

Author	Methodology	Focus	Limitation
Ao et al. [10]	Cosα method based on Debye-ring X-ray diffraction	Measured residual stress distribution in RSW stainless steel 0Cr18Ni9 nuggets.	Limited to measuring residual stress distribution; doesn't address process optimization or quality improvement directly.

Continued on next page

Table 1 continued

Liu et al. [11]	Direct finite element analysis with reverse geometric modeling	Investigated residual deformations in continuous spot welding and the influence of factors like clamping pressure and welding sequence.	Nonlinear interactions among parameters reduce the impact of individual optimizations, and results might not generalize to different geometries.
Ma et al. [12]	Combined experimental and computational approach with artificial pre-cracks	Studied LME cracks and their effects on tensile-shear strength in zinc-coated UHSS welds.	Focused on pre-crack characteristics but lacks real-world verification on natural LME cracks.
Zhao et al. [13]	Stepwise regression with dynamic resistance signals	Developed a model to predict welding quality based on dynamic resistance features.	Limited to static conditions and does not incorporate real-time adjustments or other welding types.
Burca et al. [14]	Geometrical analysis of weld nuggets	Analyzed the effect of welding parameters on nugget geometry in Nimonic80A alloy.	Focused only on geometric factors, neglecting other quality or mechanical properties.
Ye et al. [15]	Neural network-based vision inspection	Classified welding defects in electronic components using image features with a neural network.	Limited generalizability across different types of welding and products.
Yang et al. [16]	Transfer learning with GoogLeNet and MLP	Classified spot-welding products using solder joint images with high accuracy.	General performance across different products and varying conditions remains challenging.
Bacioiu et al. [17]	HDR camera with ANN for TIG welding defect assessment	Proposed a system for detecting TIG welding defects using HDR imaging and ANN.	Limited to TIG welding and does not address other defect types or welding techniques.
Chen et al. [18]	Pattern-based feature extraction with supervised ML (Random Forests)	Monitored welding penetration in pulsed GTAW using visual features.	Vulnerable to visual disturbances like spattering and arc intensity changes.
Nomura et al. [19]	CNN for quality prediction in GMAW	Predicted penetration depth and burn-through in GMAW using surface monitoring images.	Requires specific sample shapes and conditions; generalization to other setups is uncertain.
Zhang et al. [20]	Deep learning (CNN) for robotic arc welding	On-line detection of weld penetration defects with CNN-based weld image analysis.	Robustness tested under augmentation, but environmental instability could still pose challenges.
Wang et al. [21]	Tutorial on deep learning in manufacturing	Overview and case study of deep learning applications in welding, emphasizing CNN and RNN.	Introductory in nature; lacks deeper exploration of practical industrial implementation.

2 Methodology

The material utilized were CR steel sheets with an elongation of 15% and a tensile strength of 980 MPa. The material has a 1.2 mm thickness. According to ISO 10447:2015 requirements, the test specimen was created. The specimen utilized measured 100 mm in length and 55 mm in width, with a 30 mm overlap, as illustrated in Figure 1. Table 2 displays the material's chemical makeup and mechanical characteristics.

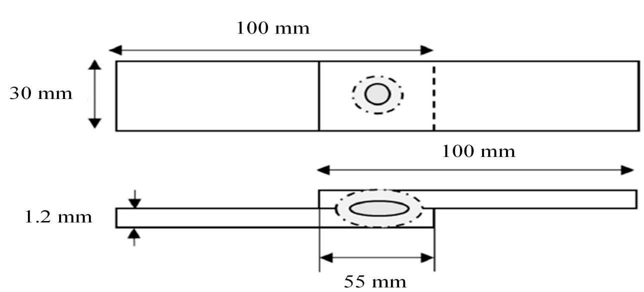

Fig 1. Geometry of welding specimen

Table 2. Chemical and mechanical properties of CR steel

Steel	Chemical composition (wt.%)				Mechanical properties		
Uncoated cold-rolled	C	Si	Elongation (%)	Yield Strength (Mpa)	Ultimate Tensile Strength (Mpa)	Elongation (%)	Yield Strength (Mpa)
	0.20	1.59	2.40	Bal.	980	15	500

Out of 10 welded specimens, five were utilized for TSS measurement and the remaining five for nugget diameter measurement. Three levels of weld current (WC) are 6, 8, and 10 kA were set. Additionally, three degrees of weld time (WT) are 10, 15 and 20 ms were specified. A fixed electrode force of 0.5 Mpa was used.

A theoretical model of the weld's surface appear is shown in Figure 2. The illumination was focused at 30° angle from vertical and was placed 2 meters away from the weld surface. The light had a white color and 1600 lumens of light are present. The vertical distance measured between the camera and the weld surface was 120 mm. The captured image had 128 × 128 pixels. The captured image was originally in color, but for this investigation, it was transformed to grayscale and utilized as input data for a quality prediction video. Every pixel in the converted grayscale image had its data values adjusted to fall between 0 and 1, with 0 serving as the minimum and 1 as the maximum values.

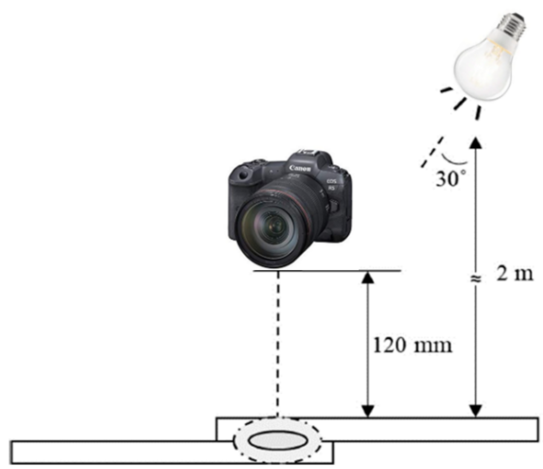

Fig 2. Condition of image data capture

2.1 HCLAN for Forecast Weld Quality

This proposed work introduced a novel "Hybrid CNN-LSTM with Attention Network" to efficiently predict the quality of the RSW. For quality prediction, this work utilized binary convolutional layers having 16 and 32 filters, respectively. The convolutional layers have a kernel size of 1 and an activation function of ELU. Next, this work built up two stacked LSTM layers with a dropout of 0.2 for another LSTM-layer and 24 neurons for each layer. It is important to note that every LSTM-layer uses ELU as the activation function. A dropout layer with a dropout rate of 0.2 is added after the stacked LSTM layers. Overfitting of the model is prevented by the dropout layer. All of the collected features eventually pass through the attention layer. The two convolution layers' filters for the quality prediction are 32 and 64, correspondingly.

2.1.1 Convolution Neural Network

The one-dimensional convolutional-layer1 receives the given data after passing across the input-layer. The kernel only advances in the path of time in this instance. The Convolution-layer1 receives the input $Y = \{y_1, y_2, \ldots y_T\}$; hence, we have

$$L = ELU(V © Y + b) \tag{1}$$

where b stands for the bias vector, V is a weight array, © indicates the convolution operation, and L is the result of the lth filter. ELU is the activation function. The outputs of the convolution process are obtained by the first Convolution-layer1 by repeating it, and they are subsequently fed into the second Convolution-layer2.

2.1.2 LSTM layers

The outcomes of the convolutional layers are received by the LTSM-layer. Three gates are present: an input gate, a forget gate and output gate. There is also a cell state. The disappearing gradient issue and the explosion gradient issue that an RNN faces are resolved by the LSTM due to its distinct cell state and three gates. The input gate picks what type of data is kept in the cell state after the forget gate chooses which information to discard in the first phase. The following are the equations:

$$g_t = \sigma(V_g.[h_{t-1}, \bar{y_t}] + b_g) \tag{2}$$

$$j_t = \sigma(V_j.[h_{t-1}, \bar{y_t}] + b_j) \tag{3}$$

$$C_t = ELU(V_C.[h_{t-1}, \bar{y_t}] + b_C) \tag{4}$$

where $\bar{y_t}$ indicates the layer's input at time t, V_* represents the weight array of the consistent gate, h_{t-1} indicates the hidden state of $t-1$, b_* indicates the bias of tierce gates, j_t is the input gate, and C_t is a candidate value. Additionally, g_t marks the forget gate. The input gate j_t and C_t can be utilized to determine how the cell state is treated at time t. Subsequently, j_t is necessary to update the current cell state $\bar{C_t}$, as it may choose to input data from C_t and forget information from C_{t-1}. Lastly, the present output is obtained by the output gate out_{put} .

$$\bar{C_t} = g_t * C_{t-1} + j_t * C_t \tag{5}$$

$$out_{put} = \sigma(V_{out}.[h_{t-1}, \bar{y_t}] + b_{out}) \tag{6}$$

$$h_t = out_{put} * ELU(\bar{C_t}) \tag{7}$$

2.1.3 Attention-Layer

Next, the weighted LSTM layers have extracted the long-term dependencies from the features, and the attention layer will use their output as its input. The additional attention layer automatically learns the significance of each concealed state. A weighted summation is a straightforward interpretation of the attention mechanism. The softmax function is then used to make sure that the total of all weights equals one after first determining how important the input attributes are. To obtain the output, the weights and the input features are increased in accordance with one another before being added together. The following equations are pertinent:

$$a_t^m = \frac{exp(e_t^m)}{\sum_{i=1}^{n} exp(e_t^i)} \tag{8}$$

$$e_t^m = w_e^T \sigma(V_e.\left[h_{t-1}, \bar{y_t}\right] + U_e h_{t+} b_e) \tag{9}$$

$$P_t = \sum_t^T a_t^T h_t \tag{10}$$

Where $w_e, b_e \in R^T$, $V_e \in R^{T \times k}$, and $U_e \in R^{k \times k}$ are attributes that essential to be learned; k is the number of neurons; a_t^m is the attention weights of the m^{th} input at time t ; e_t^m denotes the status of the h_t; and P_t is the output of attention layer gained by a weighted summary of all hidden states.

The CNN layers are first used to obtain the local features after the data has been fed into the model. Second, the first LSTM layer logs long-term dependencies between variables after receiving the CNN layers' outputs. Thirdly, all hidden states from each LSTM layer are fed into the attention layer, which has the ability to assess the relative importance of these hidden layer states. The result is ultimately determined by a weighted total.

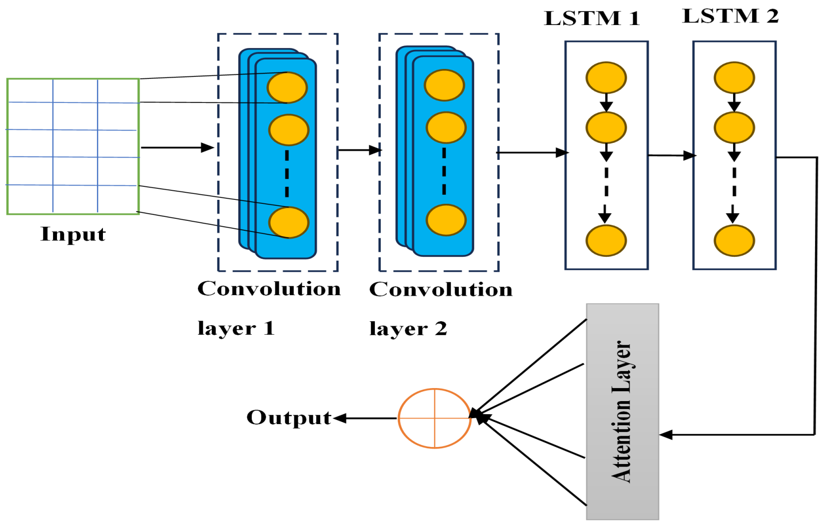

Fig 3. Hybrid CNN-LSTM with Attention layer

3 Results and discussion

3.1 Preparation of training data

In summary, the entire range of welding circumstances, as well as camera and illumination variations, yields a data set of 1080 images, which is still quite small for convolutional neural network training. In this work, the data augmentation technique was used to modify the spot-welding photos. The image was first rotated clockwise for 90, 180, and 270 degrees after being horizontally flipped. From one original photograph, a total of eight images were produced. By using this method, there are 8640 more photos in the collection. Figure 4 illustrates several examples of the visuals produced by flipping and rotating photos.

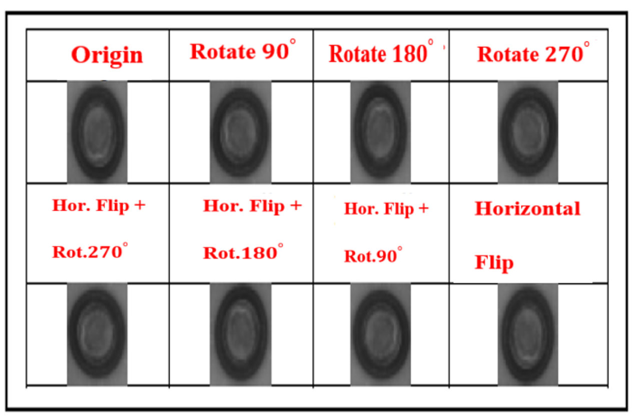

Fig 4. Data augmentation with the horizontal flip and rotation

Neural network learning is the process of using the training dataset to determine the ideal weight and bias values. In order to determine the attributes (bias and weights values) with the lowest error values among the calculated and actual outcomes, repeated learning was carried out utilizing the error calculation, as indicated by Equation (11).

$$CE = \frac{1}{2}\sum_{a}(x_a - t_a)^2 \tag{11}$$

3.2 Outcome of Welding Tests for Surface Heat Trace

The HT images of the weld surface below various welding settings are shown in Figure 5. It has been discovered that the heat markings on the specimen's surface increase with the amount of time and current the welds have. A rise in the TSS and nugget diameter is shown by the dilatation of the heat trace.

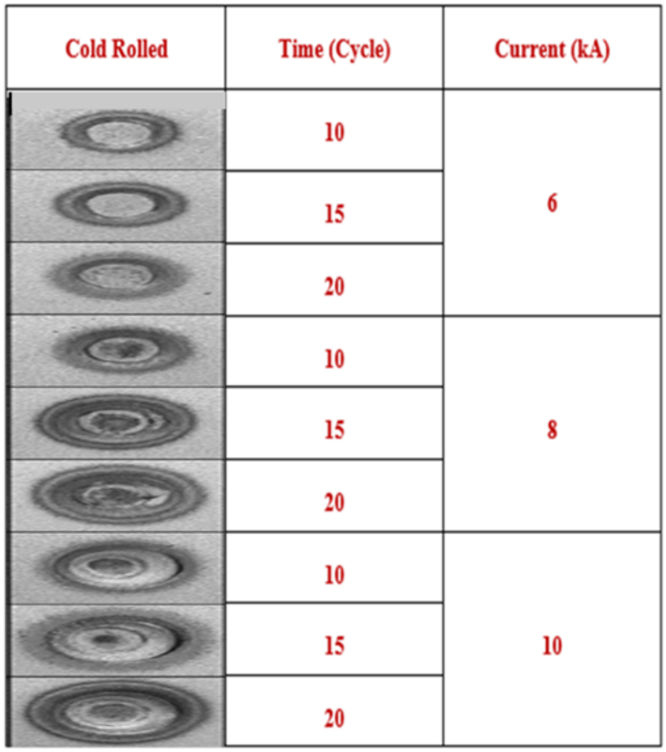

Fig 5. Images of reference welding parts for every parameter

Table 3. Spot weld-ability results for every parameter

No.	Welding condition			Measured outcome				Predicted outcome			
	Material	Current (kA)	Time (ms)	Tensile shear strength (kN)	Nugget size (mm)	Fracture mode	Expulsion	Tensile shear strength (kN)	Nugget size (mm)	Fracture mode	Expulsion
1	CR	6	10	5.3	2.6	0	0	5.3	2.6	0	0
2	CR	6	10	5.7	2.5	0	0	5.7	2.5	0	0
3	CR	6	10	5.4	2.5	0	0	5.4	2.5	0	0
4	CR	6	10	5.8	2.4	0	0	5.8	2.4	0	0
5	CR	6	10	5.5	2.5	0	0	5.5	2.5	0	0
6	CR	6	15	5.8	2.8	0	0	5.8	2.8	0	0
7	CR	6	15	6.1	2.6	0	0	6.1	2.6	0	0
8	CR	6	15	6.6	2.5	0	0	6.6	2.5	0	0
9	CR	6	15	6	2.5	0	0	6	2.5	0	0
10	CR	6	15	6	2.6	0	0	6	2.6	0	0
11	CR	8	20	6	2.9	0	0	6	2.9	0	0
12	CR	8	20	5.8	2.9	0	0	5.8	2.9	0	0
13	CR	8	20	6.4	3	0	0	6.4	3	0	0
14	CR	8	20	6.7	3	0	0	6.7	3	0	0
15	CR	8	20	6.6	3	0	0	6.6	3	0	0

Continued on next page

Table 3 continued

16	CR	8	10	12.1	4	0	0	12.1	4	0	0
17	CR	8	10	12.9	3.8	0	0	12.9	3.8	0	0
18	CR	8	10	12.3	3.7	0	0	12.3	3.7	0	0
19	CR	8	10	12.5	3.7	0	0	12.5	3.7	0	0
20	CR	8	10	12.8	4	0	0	12.8	4	0	0
21	CR	10	15	12.6	4	0	0	12.6	4	0	0
22	CR	10	15	12.8	4.1	0	0	12.8	4.1	0	0
23	CR	10	15	13	4.2	0	0	13	4.2	0	0
24	CR	10	15	12.9	4.3	0	0	12.9	4.3	0	0
25	CR	10	15	12.7	4	0	0	12.7	4	0	0
26	CR	10	20	12.5	4.2	0	0	12.5	4.2	0	0
27	CR	10	20	13.2	4.4	0	0	13.2	4.4	0	0
28	CR	10	20	13.1	4.4	0	0	13.1	4.4	0	0
29	CR	10	20	12.8	4.3	0	0	12.8	4.3	0	0
30	CR	10	20	12.5	4.4	0	0	12.5	4.4	0	0

3.3 Comparison of expected values based on welding conditions and welding quality outcomes

Table 3 displayed thereal measured values and the hybrid CNN-LSTM with AN projected value for the TSSs, fracture shapes, nugget dimensions, and ejection appearance under every welding circumstances. The interfacial fracture was designated as 0 in the fracture mode, and the button fracture as 1. Regardless of the welding period, the expulsion of the CR steel sheet happened at a welding current of 10 kA. The nugget diameter increased to 4.4 mm, and the TSS displayed a maximum of 12.5 kN.

3.4 Learning using hybrid CNN-LSTM with AN

From Table 3, the TSSs utilized in the learning process had a 98.5% prediction accuracy and a 0.9895 coefficient of determination. And also, the coefficient of determination for the nugget diameters utilized in the learning method was 0.9787, and the prediction accuracy was 97.8%. The value 0 in the fracture mode prediction denotes an interfacial fracture, while value 1 denotes a button fracture. In terms of the forecast of expulsion incidence, 0 denotes no expulsion occurrence and 1 denotes an expulsion event. Consequently, under all welding settings, the forecast accuracy of the fracture shape and the expulsion rate were 100%.

3.5 Validation of proposed predictive models

Four welding circumstances in total were chosen, and the confirmation testing was carried out 5 times under equal conditions. With the exception of the welding settings used for the learning, welding current and welding time were chosen for these four verification test conditions. The welding conditions involved 980 MPa-grade CR steel, with WC of 6 kA and 8 kA, WT of 10 ms and 15 ms, and an electrode force of 0.5 MPa. Table 4 displays the results that were measured and anticipated using the proposed model that was created throughout the learning phase in each of the 10 verification situations. The largest inaccuracy of the nuget diameter was 0.5 mm, and the highest prediction error for TSS was 1 kN. In every verification test, the fracture shape and expulsion amount were accurately predicted.

Table 4. Confirmation test results

No.	Welding condition			Measured outcomes				Predicted outcomes			
	Material	Current (kA)	Time (ms)	Tensile shear strength (kN)	Nugget size (mm)	Fracture mode	Expulsion	Tensile shear strength (kN)	Nugget size (mm)	Fracture mode	Expulsion
1	CR	6	10	5.3	2.6	0	0	5.7	2.3	0	0
2	CR	6	10	5.7	2.5	0	0	5.9	2.2	0	0
3	CR	6	10	5.4	2.5	0	0	4.2	2.8	0	0
4	CR	6	10	5.8	2.4	0	0	5.1	2.0	0	0
5	CR	6	10	5.5	2.5	0	0	4.7	2.5	0	0
6	CR	8	15	5.8	2.8	0	0	5.2	2.4	0	0
7	CR	8	15	6.1	2.6	0	0	5.8	2.7	0	0

Continued on next page

Table 4 continued

8	CR	8	15	6.6	2.5	0	0	6.1	2.9	0	0
9	CR	8	15	6	2.5	0	0	5.8	2.2	0	0
10	CR	8	15	6	2.6	0	0	6	2.5	0	0

According to Table 4, the TSS accuracy was estimated to be 97.2%, and the coefficient of determination was 0.9378. The forecast's average precision for nugget diameter was 97.1%, with a coefficient of determination of 0.787. The projected outcomes of the confirmation examinations showed that surface HT photos of the welds in RSW can be used to predict HCLAN quality prediction with a high degree of accuracy.

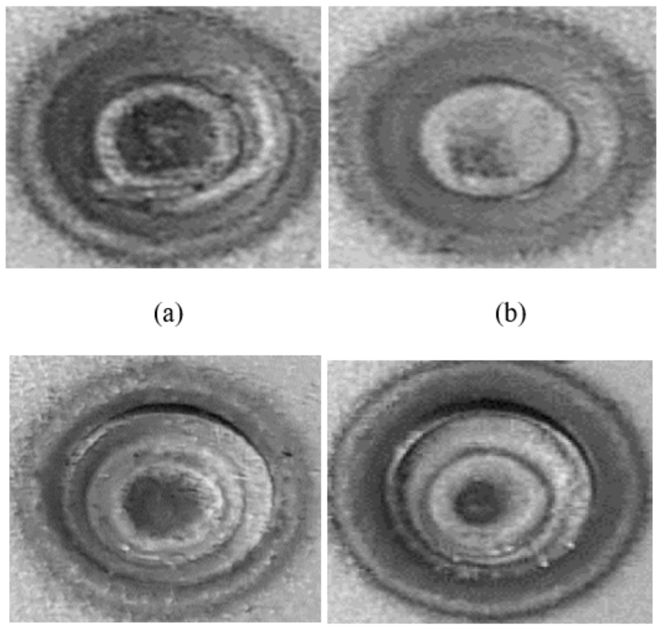

(a) (b) (c) (d)

Fig 6. Inaccurate image-CR-6kA, 10ms, (b): Normal image-CR-6kA, 15ms, (c): Inaccurate image-CR-8kA, 10ms, (d): Normal image-CR-8kA, 15ms

Figure 6 presents a surface HT image of welds with lesser prediction precision in confirmation testing. Figure 6 (**a-d**) shows data with considerable discrepancies among observed and projected values. The measured value in Figure 6 (**a, b**) was 5.8 kN, whereas the anticipated value with a 13.6% error rate was 5.1 kN. The observed value of TSS in Figure 6 (**c, d**) was 5.2 kN, even though the expected value was 6.0 kN with an error of 6.5%. The image's state may have been interpreted differently because of variations in the light circumstances between the learning phase and the verification operation. This study attempted to use surface heat trace images in RSW to estimate the quality of welds. It is feasible to estimate the resistance spot weld quality in the manufacturing line by using this prediction technique. It also lowers the fault rate and makes it possible to check the weld quality. Nevertheless, the conditions of heat transport, contamination of the electrodes, electrode slope, misalignment, etc., affect the surface heat trace images. For the purpose of making an accurate prediction, it is crucial to take an image under identical photographic conditions. Future research will address the prediction of weld quality in the event that the previously indicated picture condition is poor or erroneous. Additionally, this study applies hybrid CNN-LSTM with AN to base material and welding circumstances under particular parameters to forecast the weld quality. By improving the weight between nodes through additional learning, which is believed that precise welding quality may be predicted in cases where the kind, thickness, and welding conditions differ.

3.6 Comparative Analysis

In this study, the hybrid CNN-LSTM with Attention Network (HCLAN) model was compared to various existing methods for resistance spot weld (RSW) quality prediction and defect detection. The results indicate that the HCLAN model excels in terms of accuracy and prediction capabilities for multiple weld quality parameters like tensile shear strength (TSS), nugget diameter, fracture mode, and expulsion. In contrast to previous studies that used traditional methods (e.g., ultrasonic C-scan testing[22]) or deep learning approaches like Faster R-CNN[23] and YOLOv3[24], our method offers a significant improvement in prediction precision. While methods such as Faster R-CNN achieved over 90% detection accuracy, they were primarily focused on defect detection, and not on predicting detailed quality attributes such as TSS and nugget size. Our model, leveraging hybrid CNN-LSTM architecture with an attention mechanism, achieved near-perfect accuracy (100%) for weld fracture mode and expulsion detection and offered high prediction accuracy for other metrics (e.g., TSS prediction with 98.5% accuracy).

3.7 Limitations and Biases

The study acknowledges some limitations in its methodology, primarily related to training data and environmental factors. The relatively small dataset (1080 images) might lead to overfitting, and although data augmentation was used to address this issue, the model's performance might still degrade under conditions that deviate significantly from the training setup (e.g., varying lighting or misalignment of the camera). Another limitation is the reliance on visual input data, which, while powerful, is still susceptible to quality variation in the weld images due to environmental influences. The biases in the data may arise if certain welding conditions are underrepresented in the training data, potentially leading to reduced accuracy in rare or unseen welding conditions. These limitations may slightly impact the validity and reliability of the predictions, particularly in industrial environments where weld conditions are highly variable.

3.8 Theoretical Contributions

The research contributes to the theoretical frameworks of weld quality prediction and deep learning by integrating hybrid CNN and LSTM networks with attention mechanisms. Previous works in this domain primarily utilized CNNs or LSTMs independently or in simpler configurations. This paper's novel approach of combining these with attention mechanisms introduces a new theoretical insight into how attention can be effectively used to focus on key weld features in heat trace images, leading to better predictive performance. This approach enhances the interpretability of the model, as attention mechanisms allow the model to focus on important regions of the image that are most relevant to the welding quality. The theoretical contribution also extends into the realm of multimodal welding data, where temporal (LSTM) and spatial (CNN) data are combined to provide a richer understanding of the welding process.

3.9 Practical Implications

The practical implications of this research are significant for real-time industrial quality control in resistance spot welding. The proposed method can be easily implemented in manufacturing environments where automation is critical, such as in the automotive industry. The high accuracy and speed of the hybrid model (with a prediction error of only 2.8% for nugget diameter and 2.3% for TSS) make it a viable candidate for real-time monitoring systems. This can potentially replace manual inspection methods, reducing human error and increasing operational efficiency. Additionally, the predictive nature of the model allows for early detection of potential weld issues such as expulsion or poor fracture modes, enabling timely corrective actions and minimizing waste or defects in production.

4 Conclusion

This study developed an advanced automated methodology for predicting resistance spot weld quality using heat trace images, leveraging a Hybrid CNN-LSTM with Attention Network (HCLAN). Key achievements include prediction errors of 2.8% for nugget diameter and 2.3% for tensile shear strength, with a perfect accuracy rate of 100% for identifying weld fracture modes and ejection occurrences. These results validate the model's high effectiveness in interpreting weld surface patterns and forecasting weld quality.

Novelty: The HCLAN framework uniquely integrates CNN and LSTM architectures with attention mechanisms, providing an innovative and efficient tool for industrial applications. By automating weld quality inspection, this study addresses limitations of conventional methods, reducing dependency on manual evaluation and minimizing errors.

Prospects: Future work could extend this approach to accommodate various materials and welding parameters, enabling real-time monitoring and adaptive quality control in dynamic manufacturing environments.

Recommendations: Further research should explore scaling the method to inline weld inspection systems, assessing its applicability in multi-material assemblies, and integrating it with Industry 4.0 frameworks to optimize welding operations.

References

1) Soomro IA, Pedapati SR, Awang M. A review of advances in resistance spot welding of automotive sheet steels: emerging methods to improve joint mechanical performance. *The International Journal of Advanced Manufacturing Technology*. 2022;118:1335–1366. Available from: https://doi.org/10.1007/s00170-021-08002-5.
2) Zhao D, Bezgans Y, Wang Y, Du W, Vdonin N. Research on the correlation between dynamic resistance and quality estimation of resistance spot welding. *Measurement*. 2021;168. Available from: https://doi.org/10.1016/j.measurement.2020.108299.
3) Zhao D, Ivanov M, Wang Y, Du W. Welding quality evaluation of resistance spot welding based on a hybrid approach. *Journal of Intelligent Manufacturing*. 2021;32(7):1819–1832. Available from: https://link.springer.com/article/10.1007/s10845-020-01627-5.
4) Das T, Paul J. Interlayers in resistance spot-welded lap joints: A critical review. *Metallography, Microstructure, and Analysis*. 2021;10:3–24. Available from: https://doi.org/10.1007/s13632-021-00714-0.
5) Choi SG, Hwang I, Kim YM, Kang B, Kang M. Prediction of the weld qualities using surface appearance image in resistance spot welding. *Metals*. 2019;9(8). Available from: https://doi.org/10.3390/met9080831.
6) Dai W, Li D, Tang D, Jiang Q, Wang D, Wang H, et al. Deep learning assisted vision inspection of resistance spot welds. *Journal of Manufacturing Processes*. 2021;62:262–274. Available from: https://doi.org/10.1016/j.jmapro.2020.12.015.
7) Haghshenas N, Moshayedi H. Monitoring of resistance spot welding process. *Experimental Techniques*. 2020;44:99–112. Available from: https://doi.org/10.1007/s40799-019-00341-z.
8) Summerville C, Compston P, Doolan M. A comparison of resistance spot weld quality assessment techniques. *Procedia Manufacturing*. 2019;29:305–317. Available from: https://doi.org/10.1016/j.promfg.2019.02.142.
9) Taram A, Roquelet C, Meilland P, Dupuy T, Kaczynski C, Bodnar JL, et al. Nondestructive testing of resistance spot welds using eddy current thermography. *Applied optics*. 2018;57(18):63–68. Available from: https://doi.org/10.1364/AO.57.000D63.
10) Ao S, Li C, Huang Y, Luo Z. Determination of residual stress in resistance spot-welded joint by a novel X-ray diffraction. *Measurement*. 2020;161. Available from: https://doi.org/10.1016/j.measurement.2020.107892.
11) Liu X, Wei Y, Wu H, Zhang T. Factor analysis of deformation in resistance spot welding of complex steel sheets based on reverse engineering technology and direct finite element analysis. *Journal of Manufacturing Processes*. 2020;57:72–90. Available from: https://doi.org/10.1016/j.jmapro.2020.06.028.
12) Ma Y, Yu Y, Geng P, Ihara R, Maeda K, Suzuki R, et al. Fracture modeling of resistance spot welded ultra-high-strength steel considering the effect of liquid metal embrittlement crack. *Materials & Design*. 2021;210. Available from: https://doi.org/10.1016/j.matdes.2021.110075.
13) Zhao D, Bezgans Y, Wang Y, Du W, Vdonin N. Research on the correlation between dynamic resistance and quality estimation of resistance spot welding. *Measurement*. 2021;168. Available from: https://doi.org/10.1016/j.measurement.2020.108299.
14) Burca L, Mitelea I, Utu ID, Burca M. Resistance spot welding particularities of the nickel alloy Nimonic 80 A. In: and others, editor. Materials Today: Proceedings;vol. 45. 2021;p. 4122–4127. Available from: https://www.sciencedirect.com/science/article/abs/pii/S2214785320395468.
15) Ye S, Guo Z, Zheng P, Wang L, Lin C. A vision inspection system for the defects of resistance spot welding based on neural network. In: Liu M, Chen H, Vincze M, editors. Computer Vision Systems: 11th International Conference;vol. 10528. Springer International Publishing. 2017;p. 161–168. Available from: https://link.springer.com/chapter/10.1007/978-3-319-68345-4_14.
16) Yang Y, Zheng P, He H, Zheng T, Wang L, He S. An evaluation method of acceptable and failed spot welding products based on image classification with transfer learning technique. In: and others, editor. the 2nd International Conference. 2018;p. 1–6. Available from: https://www.researchgate.net/publication/328378475_An_Evaluation_Method_of_Acceptable_and_Failed_Spot_Welding_Products_Based_on_Image_Classification_with_Transfer_Learning_Technique.
17) Bacioiu D, Melton G, Papaelias M, Shaw R. Automated defect classification of Aluminium 5083 TIG welding using HDR camera and neural networks. *Journal of Manufacturing Processes*. 2019;45:603–616. Available from: https://doi.org/10.1016/j.jmapro.2019.07.020.
18) Chen C, Lv N, Chen S. Welding penetration monitoring for pulsed GTAW using visual sensor based on AAM and random forests. *Journal of Manufacturing Processes*. 2021;63:152–162. Available from: https://doi.org/10.1016/j.jmapro.2020.04.005.
19) Nomura K, Fukushima K, Matsumura T, Asai S. Burn-through prediction and weld depth estimation by deep learning model monitoring the molten pool in gas metal arc welding with gap fluctuation. *Journal of Manufacturing Processes*. 2021;61:590–600. Available from: https://doi.org/10.1016/j.jmapro.2020.10.019.
20) Zhang Z, Wen G, Chen S. Weld image deep learning-based on-line defects detection using convolutional neural networks for Al alloy in robotic arc welding. *Journal of Manufacturing Processes*. 2019;45:208–216. Available from: https://dx.doi.org/10.1016/j.jmapro.2019.06.023.
21) Wang Q, Jiao W, Wang P, Zhang Y. A tutorial on deep learning-based data analytics in manufacturing through a welding case study. *Journal of Manufacturing Processes*. 2021;63:2–13. Available from: https://doi.org/10.1016/j.jmapro.2020.04.044.
22) Yang L, Chuai R, Cai G, Xue D, Li J, Liu K, et al. Ultrasonic Non-Destructive Testing and Evaluation of Stainless-Steel Resistance Spot Welding Based on Spiral C-Scan Technique. *Sensors*. 2024;24(15). Available from: https://dx.doi.org/10.3390/s24154771.
23) Liu W, Hu J, Qi J. Resistance Spot Welding Defect Detection Based on Visual Inspection: Improved Faster R-CNN Model. 2024;p. 1–14. Available from: https://www.researchgate.net/publication/385092605_Resistance_Spot_Welding_Defect_Detection_Based_on_Visual_Inspection_Improved_Faster_R-CNN_Model.
24) Dai W, Li D, Tang D, Jiang Q, Wang D, Wang H, et al. Deep learning assisted vision inspection of resistance spot welds. *Journal of Manufacturing Processes*. 2021;62:262–274. Available from: https://dx.doi.org/10.1016/j.jmapro.2020.12.015.